Ca^{2+}-binding proteins tune Ca^{2+}-feedback to $Ca_V1.3$ channels in mouse auditory hair cells

Guiying Cui[1], Alexander C. Meyer[2], Irina Calin-Jageman[1], Jakob Neef[2], Françoise Haeseleer[3], Tobias Moser[2] and Amy Lee[1]

[1]*Department of Pharmacology and Center for Neurodegenerative Disease, Emory University, Atlanta, GA 30322, USA*
[2]*Department of Otolaryngology, Center for Molecular Physiology of the Brain and Bernstein Center for Computational Neuroscience, University of Göttingen, Göttingen, Germany*
[3]*Department of Opthalmology, University of Washington, Seattle, WA 98195, USA*

Sound coding at the auditory inner hair cell synapse requires graded changes in neurotransmitter release, triggered by sustained activation of presynaptic $Ca_V1.3$ voltage-gated Ca^{2+} channels. Central to their role in this regard, $Ca_V1.3$ channels in inner hair cells show little Ca^{2+}-dependent inactivation, a fast negative feedback regulation by incoming Ca^{2+} ions, which depends on calmodulin association with the Ca^{2+} channel α_1 subunit. Ca^{2+}-dependent inactivation characterizes nearly all voltage-gated Ca^{2+} channels including $Ca_V1.3$ in other excitable cells. The mechanism underlying the limited autoregulation of $Ca_V1.3$ in inner hair cells remains a mystery. Previously, we established calmodulin-like Ca^{2+}-binding proteins in the brain and retina (CaBPs) as essential modulators of voltage-gated Ca^{2+} channels. Here, we demonstrate that CaBPs differentially modify Ca^{2+} feedback to $Ca_V1.3$ channels in transfected cells and explore their significance for $Ca_V1.3$ regulation in inner hair cells. Of multiple CaBPs detected in inner hair cells (CaBP1, CaBP2, CaBP4 and CaBP5), CaBP1 most efficiently blunts Ca^{2+}-dependent inactivation of $Ca_V1.3$. CaBP1 and CaBP4 both interact with calmodulin-binding sequences in $Ca_V1.3$, but CaBP4 more weakly inhibits Ca^{2+}-dependent inactivation than CaBP1. Ca^{2+}-dependent inactivation is marginally greater in inner hair cells from CaBP4$^{-/-}$ than from wild-type mice, yet CaBP4$^{-/-}$ mice are not hearing-impaired. In contrast to CaBP4, CaBP1 is strongly localized at the presynaptic ribbon synapse of adult inner hair cells both in wild-type and CaBP4$^{-/-}$ mice and therefore is positioned to modulate native $Ca_V1.3$ channels. Our results reveal unexpected diversity in the strengths of CaBPs as Ca^{2+} channel modulators, and implicate CaBP1 rather than CaBP4 in conferring the anomalous slow inactivation of $Ca_V1.3$ Ca^{2+} currents required for auditory transmission.

(Received 2 August 2007; accepted after revision 15 October 2007; first published online 18 October 2007)
Corresponding author A. Lee: Department of Pharmacology, Emory University School of Medicine, 5123 Rollins Research Bldg, 1510 Clifton Road, Atlanta, GA 30322, USA and T. Moser: InnerEarLab, Department of Otolaryngology, Göttingen University Medical School, Center for Molecular Physiology of the Brain, Bernstein Center for Computational Neurosciences, 37099 Göttingen, Germany. Email: alee@pharm.emory.edu and tmoser@gwdg.de

In the cochlea, $Ca_V1.3$ voltage-gated Ca^{2+} channels are essential for the proper development and function of inner hair cells (IHCs) as mechanosensory transducers of acoustic stimuli. $Ca_V1.3$ channels mediate L-type Ca^{2+} currents that trigger exocytosis of neurotransmitter from IHCs onto auditory nerve afferents (Platzer *et al.* 2000; Brandt *et al.* 2003, 2005) and Ca^{2+} action potentials in IHCs before the onset of hearing (Brandt *et al.* 2003; Marcotti *et al.* 2003). Mice lacking $Ca_V1.3$ are congenitally deaf (Platzer *et al.* 2000; Dou *et al.* 2004), illustrating how factors that regulate these channels can affect sound coding at this first synapse in the auditory pathway.

Most features of IHC $Ca_V1.3$ channels, including their fast activation kinetics and relatively negative thresholds for activation, are reproduced in recombinant systems (Xu & Lipscombe, 2001; Koschak *et al.* 2001). However, $Ca_V1.3$ Ca^{2+} currents in IHCs show considerably less Ca^{2+}-dependent inactivation (CDI) than in transfected cells (Platzer *et al.* 2000; Xu & Lipscombe, 2001; Koschak *et al.* 2001). CDI is manifest as faster inactivation of Ca^{2+}

G. Cui and A. C. Meyer contributed equally to the work. This paper has online supplemental material.

DOI: 10.1113/jphysiol.2007.142307

currents (I_{Ca}) than Ba^{2+} currents (I_{Ba}) and depends on calmodulin binding to the IQ domain in the C-terminal domain of the pore-forming Ca_v1 α_1-subunit (Qin *et al.* 1999; Peterson *et al.* 1999; Zühlke *et al.* 1999). Mutations of the IQ domain in the $Ca_v1.3$ α_1-subunit ($\alpha_1 1.3$) inhibit CDI, and a $\alpha_1 1.3$ splice variant lacking the IQ domain was identified in the cochlea (Shen *et al.* 2006). However, this $\alpha_1 1.3$ variant is expressed mainly in outer hair cells (OHCs) and not IHCs, suggesting an alternative mechanism for the limited CDI of native $Ca_v1.3$ channels in IHCs.

We have shown previously that Ca^{2+} binding proteins related to calmodulin (CaBP1 and CaBP4) can physically displace calmodulin from Ca_v channels, but with distinct functional consequences (Lee *et al.* 2002; Zhou *et al.* 2004; Haeseleer *et al.* 2004; Zhou *et al.* 2005). CaBP1 is expressed primarily in the brain and retina and abolishes CDI of $Ca_v1.2$ channels (Zhou *et al.* 2004, 2005). CaBP4 is localized in photoreceptor nerve terminals, where its association with $Ca_v1.4$ causes the channels to activate at more hyperpolarized membrane potentials required for normal visual transduction (Haeseleer *et al.* 2004). Considering the analogous functions of $Ca_v1.3$ in IHCs and $Ca_v1.4$ in photoreceptors, we hypothesized that CaBP4 might be expressed in IHCs and confer the native phenotype of $Ca_v1.3$ Ca^{2+} current in these cells. Evidence favouring this hypothesis was provided in a recent study (Yang *et al.* 2006). Here, we further investigated the role of CaBPs in the regulation of $Ca_v1.3$ Ca^{2+} currents in IHCs. Our results show that CaBP4 has relatively minor effects on $Ca_v1.3$ CDI, which alone cannot account for the slowly inactivating properties of $Ca_v1.3$ in IHCs. Instead, the data implicate CaBP1 as a key candidate for regulating CDI in IHCs.

Methods

Ethical approval

All procedures involving animals were approved by the Institutional Animal Care and Use Committee at Emory University in accordance with National Institutes of Health guidelines and animal welfare guidelines at the University of Göttingen and the State of Lower Saxony. After killing the mice by cervical dislocation the skull was opened, and the cochlea was removed and opened at the apex so that the apical coil could be harvested for immuncytochemical or electrophysiological experiments.

Constructs and molecular biology

The following Ca_v subunit cDNAs were used: $\alpha_1 1.3$ containing exon 42 (GenBank no. AF370009 and AF370010 for additional sequence encoded by exon 42), β_{1b} (GenBank no. NM017346), $\alpha_1 1.2$ (GenBank no. M67515), β_{2A} (GenBank no. NM053581), β_3 (GenBank no. NM012838), β_4 (GenBank no. L02315), and $\alpha_2\delta$ (GenBank no. M21948). FLAG-$\alpha_1 1.3$ and GST (glutathione-*S*-transferase)-tagged $\alpha_1 1.3$ C-terminal construct (GST-$\alpha_1 1.3$ CT: nucleotides 5886–6465) were previously described (Calin-Jageman *et al.* 2007). The I-E mutation was introduced at position 1608 in $\alpha_1 1.3$ and CT by quick-change mutagenesis with specific oligonucleotide primers. GST-NT corresponds to amino acids 1–117 of $\alpha_1 1.3$ subcloned into *Bam*HI/*Not*I sites of pGEX4T-1. CaBP1, CaBP2, CaBP4 and CaBP5 constructs used for mammalian cell expression were previously described (Haeseleer *et al.* 2004; Zhou *et al.* 2004).

Cell culture, transfection, and lysate preparation

Culture and transfection of HEK293T cells by Geneporter transfection reagent (Genlantis, San Diego, CA, USA) was as previously described (Calin-Jageman *et al.* 2007). For immunoprecipitation, HEK293T cells were transfected with cDNAs encoding $Ca_v1.3$ (FLAG-$\alpha_1 1.3$ (6 μg), β_{2A}, and $\alpha_2\delta$ (2 μg each) with or without CaBP4 (2 μg). For electrophysiological experiments, HEK293T cells plated on 35 mm dishes were transfected with $\sim$3 μg total DNA (FLAG-$\alpha_1 1.3$ or FLAG-$\alpha_1 1.2$ (1.5 μg), β (0.8 μg), $\alpha_2\delta$ (0.8 μg) $\pm$ GFP-tagged CaBP1 (0.1 μg), GFP-tagged or untagged CaBP4 (0.1 μg) or GFP expression plasmid (0.01 μg)). These transfection conditions have been optimized to compensate for the inhibitory effect of CaBPs on Ca_v current density, and yield measurable whole-cell currents (0.1−0.5 nA) that are easily amenable to biophysical analysis. For electrophysiological recording, GFP fluorescence was used to identify cells cotransfected with Ca_v1 subunits and CaBPs. Due to the inherently weak fluorescence associated with the GFP-tagged CaBP4 construct, we generally used untagged CaBP4 in combination with GFP expression plasmid (0.01 μg) for detection of cotransfected cells. Since there was no significant difference in the effects of GFP-CaBP4 or untagged CaBP4, data resulting from both transfection methods were pooled.

Binding and coimmunoprecipitation assays

Methods for pull-down of CaBP1 or CaBP4 from transfected HEK293T cell lysates by GST-$\alpha_1 1.3$ proteins immobilized on beads were published previously (Zhou *et al.* 2005; Zhou *et al.* 2004). Co-immunoprecipitation of $Ca_v1.3$ and CaBP4 from transfected HEK293T cells was also as previously described (Calin-Jageman *et al.* 2007). Western blotting was performed with appropriate antibodies (CaBP1 1 : 1000, CaBP4 1 : 2000) followed by HRP-conjugated anti-rabbit antibodies (1 : 2000) and enhanced chemiluminescent detection reagents (Amersham Biosciences, Piscataway, NJ, USA).

Immunohistochemistry

For Figs 1*A* and *B* and 5*B*, *C* and *E* and online supplemental material Supplemental Fig. 1*b* (CaBP2 and CaBP5), immunostaining and confocal analysis of whole-mount mouse organ of Corti (P14–15, P28, or 2 months old as indicated) were performed essentially as described (Sendin *et al.* 2007). The following antibodies were used: mouse anti-CtBP2 IgG1 (1 : 200; BD Biosciences, San Jose, CA, USA), anti-CaBP2, 4 and 5 (1 : 400 (Haeseleer *et al.* 2000) and AlexaFluor488- and AlexaFluor568-labelled secondary antibodies (1 : 200; Invitrogen, Carlsbad, CA, USA). For Fig. 5*A* and Supplemental Fig. 1*a* and *b* (CaBP1), cochleae were fixed with 4% paraformaldehyde/phosphate-buffered saline (PBS) and decalcified with 10% EDTA/PBS for 24 h prior to immunostaining with rabbit anti-CaBP1 or CaBP4 antibodies (Haeseleer *et al.* 2000; 1 : 500) and FITC donkey anti-rabbit IgG (1 : 200; Jackson ImmunoResearch, West Grove, PA, USA). Before mounting, most samples were incubated in Hoechst 34580 (1 : 1000, Invitrogen) for 5–10 min. Confocal images were acquired using a Leica SP2 or SP5 (Leica Microsystems, Mannheim, Germany) or Zeiss LSM 510 laser scanning confocal microscope. Processed images were assembled for display in Adobe Photoshop and Illustrator or Macromedia Freehand software.

RT-PCR

RNA was isolated from mouse (P14) cochlea with Trizol reagent (Invitrogen) and subject to RT-PCR with primers specific for CaBP1, 2, 4, or 5. Amplification of CaBP1 was performed with standard primers, while that for CaBP2, 4, and 5 required nested primers. Amplicons were analysed on agarose gels and were detected alongside negative control reactions that lacked reverse transcriptase. The following primer sets were used: CaBP1 forward: GACAAAGACAAGGATGGTTAC, reverse: CTCTTCAA-AGTCCACTCGTCC; CaBP2 forward 1: ATGGTTCAG-AGACCCATGG, reverse 1: CCGAGACATCATCCGA-ACAAA, forward 2: GCATGCATCTTCCTTCGACCC, reverse 2: GGTCAATGTCTTGGAGTATC; CaBP4 forward 1: GAGTTTGACACTGACCAGGAC, reverse 1: CTCGTC-AAAGTCTATGGTGC, forward 2: CAGCACGTGAAG-ATGCGCATG, reverse 2: CAACATCTCATCCAGTTCA-GTG; CaBP5 forward 1: ATGCAGTTTCCAATGGGTC-CTG, reverse 1: CGAGACATCATCTTCACAAACA, forward 2: CAGGATGAGCTTGATGAGCTC, reverse 2: TGCTGCAG TTCT GCCAGTGT.

Electrophysiology

Electrophysiological data were acquired with EPC-9 patch-clamp amplifiers driven by Pulse software (HEKA Elektronik, Lambrecht/Pfalz, Germany) and analysed with Igor Pro software (Wavemetrics, Lake Oswego, OR, USA). For transfected HEK293T cells, extracellular recording solutions contained (mM): 150 Tris, 1 $MgCl_2$, and 10 $BaCl_2$ or 10 $CaCl_2$. Intracellular solutions consisted of (mM): 140 *N*-methyl-D-glucamine, 10 Hepes, 2 $MgCl_2$, 2 Mg-ATP, and 5 EGTA. The pH of intracellular and extracellular recording solutions was adjusted to 7.3 with methanesulphonic acid. Electrode resistances were typically 1–2 MΩ in the bath solution, and series resistance was ∼2–4 MΩ, compensated up to 80%. Current density was measured by dividing the amplitude of the Ca^{2+} current by the cell capacitance. For this purpose, the Ca^{2+} current was evoked by −90 to −20 mV (for $Ca_v1.3$), −80 to −10 mV (for $Ca_v1.2$), and −90 to +10 mV (for $Ca_v1.3$I-E). For analysis of *I–V* curves, currents were evoked by 20 ms pulses to varying test voltages from a holding voltage of −90 mV. Current amplitudes were plotted against test voltage and fitted with the Boltzmann function:

$$g(V - E)/\{1 + \exp[(V - V_{1/2})/k] + b\}$$

where g is the maximum conductance, V is the test potential, E is the apparent reversal potential, $V_{1/2}$ is the potential of half-activation, k is the slope factor, and b is the baseline. Statistical comparisons were by t test.

For IHCs, perforated patch-clamp recordings were made from the apical coil of freshly dissected organs of Corti from NMRI, C57Bl/6, or $CaBP4^{-/-}$ mice (2–4 weeks of age) at the basolateral face of IHCs at room temperature. The intracellular recording solutions contained (mM), for exocytosis: 140 caesium gluconate, 13 TEA-Cl, 10 CsOH-Hepes; for CDI: 130 caesium gluconate, 10 TEA-Cl, 10 4-AP, 10 NaOH-Hepes, 1 $MgCl_2$. Both solutions contained amphotericin B (250 $\mu g\,ml^{-1}$). The extracellular solutions contained (mM), for exocytosis: 105 NaCl, 35 TEA-Cl, 2.8 KCl, 2 $CaCl_2$, 1 $MgCl_2$, 10 NaOH-Hepes, 10 D-glucose; for CDI: 104 NaCl, 35 TEA-Cl, 2.8 KCl, 1 $MgCl_2$, 1 CsCl, 5 4-AP, 10 NaOH-Hepes, 10 D-glucose and 5 Ca^{2+} or 5 Ba^{2+}. All solutions were adjusted to pH 7.2. With these solutions, electrode resistances were typically 4–6 MΩ. All voltages were corrected for liquid junction potentials. C_m was measured as previously described (Moser & Beutner, 2000) and ΔC_m was estimated as the difference between the mean C_m over 60–400 ms after the end of the depolarization and the mean prepulse capacitance (400 ms). Integrals of the Ca^{2+} current were calculated from the total depolarization-evoked inward current, including Ca^{2+} tail currents after leak subtraction. Cells with a membrane current exceeding −50 pA at the standard holding potential of −86 mV were discarded from the analysis.

All averaged data are presented as the mean ± S.E.M. Statistical significance of differences between two groups was determined by Student's t test or ANOVA as indicated (SigmaStat, Systat Software Inc., San Jose, CA, USA).

In vivo analysis of auditory function in CaBP4$^{+/-}$ and CaBP4$^{-/-}$ mice

The development and characterization of CaBP4$^{-/-}$ mice were previously described (Haeseleer *et al.* 2004). For auditory brainstem responses (ABR) and distortion product otoacoustic emissions (DPOAE), mice (4 weeks old) were measured essentially as previously described (Khimich *et al.* 2005). Briefly, for ABR, tone bursts (4/6/8/12/16/24/32 kHz, 10 ms plateau, 1 ms rise/fall) or clicks (of 0.03 ms) were applied in the free field at 20 Hz (System 2, Tucker-Davis Technology, Gainesville, FL, USA and high frequency speaker: Monacor International, Bremen, Germany). Intensities are displayed as sound pressure level (dB root mean square for tone bursts, dB peak equivalent for clicks). Thresholds were estimated with 10 dB precision by visual inspection of average ABR traces.

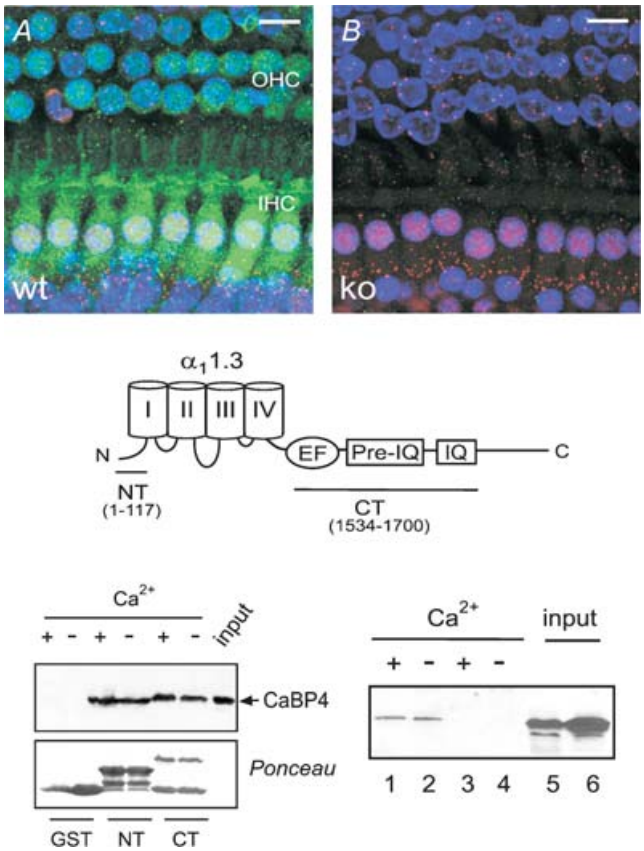

Figure 1. CaBP4 is localized in IHCs and functionally interacts with Ca$_v$1.3.
A, immunofluorescence of CaBP4 in the organ of Corti from WT (*A*) and CaBP4$^{-/-}$ (*B*) mice. Projections of confocal sections show immunofluorescence for CaBP4 (green) and CtBP2/RIBEYE (red) in IHCs and OHCs. Hoechst staining (blue) marks cell nuclei. Scale bars, 10 μm. Results shown are representative of at least 2 experiments performed with 6 organs of Corti. *C*, schematic diagram of Ca$_v$1.3 α_1 subunit indicating CT and NT fragments used for binding assays with CaBP4. *D*, CaBP4 pull-down with GST-tagged CT or NT. GST or GST-CT or NT was immobilized on glutathione beads and incubated with lysates from HEK293T cells transfected with CaBP4 in the presence (+) or absence of (–) of Ca^{2+}. Bound CaBP4 was detected by Western blot with CaBP4 antibodies (top). Input represents ~5% of protein used in assay. Ponceau staining shows levels of GST proteins used in assay. Results shown are representative of 3 experiments.
E, co-immunoprecipitation of CaBP4 with Ca$_v$1.3. HEK293T cells were transfected with Ca$_v$1.3 + CaBP4 (lanes 1, 2, 5) or with CaBP4 alone (lanes 3, 4, 6), lysed, and subjected to immunoprecipitation with Ca$_v$1.3 antibodies with (+) or without (–) Ca^{2+}. Input represents ~5% of lysate used for assay. Co-immunoprecipitated CaBP4 was detected by Western blot with CaBP4 antibodies. Results shown are representative of three experiments.

Results

CaBP4 interactions with Ca$_v$1.3

By immunohistochemistry, CaBP4 was expressed in both IHCs and OHCs after the onset of hearing (Fig. 1*A*), while it was absent early in development (P0, data not shown). Within P15 IHCs, CaBP4 labelling was distributed throughout the soma (Fig. 1*A*), which was also the case at later ages (P28; online supplemental material, Supplemental Fig. 1*a*). CaBP4 immunofluorescence was not restricted to presynaptic sites, identified by double-labelling with antibodies against CtBP2 (Fig. 1*A*). The absence of CaBP4 immunofluorescence in IHCs from CaBP4$^{-/-}$ mice (Fig. 1*B* and Supplemental Fig. 1*a*) confirmed the specificity of the antibodies for detecting CaBP4 in cochlear tissue.

Next, we tested if CaBP4 directly interacts with Ca$_v$1.3 in pull-down assays with GST-tagged fragments of $\alpha_1$1.3. We focused on the cytoplasmic N-terminal (NT) and C-terminal (CT) domains of $\alpha_1$1.3 (Fig. 1*C*), since they serve as the primary CaBP interaction sites in other Ca$_v$ α_1 subunits (Lee *et al.* 2002; Haeseleer *et al.* 2004; Zhou *et al.* 2004, 2005). In these experiments, CaBP4 associated with NT and CT, but not the GST control both in the presence and absence of Ca^{2+} (Fig. 1*D*). Ca^{2+}-independent association of CaBP4 with the intact channel was also shown by coimmunoprecipitation from lysates of HEK293T cells (Fig. 1*E*). Together with previous findings that CaBP1 and CaBP4 do not require Ca^{2+} for binding to Ca$_v$ channels (Lee *et al.* 2002; Haeseleer *et al.* 2004; Zhou *et al.* 2004; Zhou *et al.* 2005), these results suggest that CaBPs are constitutive subunits of Ca$_v$ channels under basal Ca^{2+} conditions.

Since the NT and CT are modulatory sites for CDI in Ca$_v$1.2 (Ivanina *et al.* 2000; Zhou *et al.* 2005), we tested if CaBP4 binding to these regions affects CDI of Ca$_v$1.3. Inactivation was measured as I_{res}/I_{pk}, which was the current amplitude at the end of a 300 ms test pulse normalized to the peak current amplitude. CDI was calculated as the difference between I_{res}/I_{pk} for I_{Ca} and I_{Ba}. CaBP4 caused a small but significant inhibition of CDI (~13% compared to Ca$_v$1.3 alone, $P < 0.0001$; Fig. 2*A*).

CaBP4 inhibited inactivation of I_{Ca} ($I_{res}/I_{pk} = 0.21 \pm 0.02$ for $Ca_v1.3$ + CaBP4 *versus* 0.14 ± 0.01 for $Ca_v1.3$ alone; $P < 0.001$) but not I_{Ba} ($I_{res}/I_{pk} = 0.91 \pm 0.02$ for $Ca_v1.3$ + CaBP4 *versus* 0.95 ± 0.01 for $Ca_v1.3$ alone; $P = 0.06$), indicating a selective effect on CDI. However, CDI was still quite prominent in cells cotransfected with CaBP4 and $Ca_v1.3$ (Fig. 2*A*). CaBP4 also caused a modest inhibition of CDI for $Ca_v1.2$ (Fig. 2*A*), but this was in contrast to the complete blockade of $Ca_v1.2$ CDI caused by CaBP1 (Zhou *et al.* 2005; Zhou *et al.* 2004).

In these experiments and as noted previously (Yang *et al.* 2006), CaBP4 also significantly inhibited $Ca_v1.3$ current density (Table 1). If CDI of $Ca_v1.3$ depended on global Ca^{2+} signals resulting from multiple open channels,

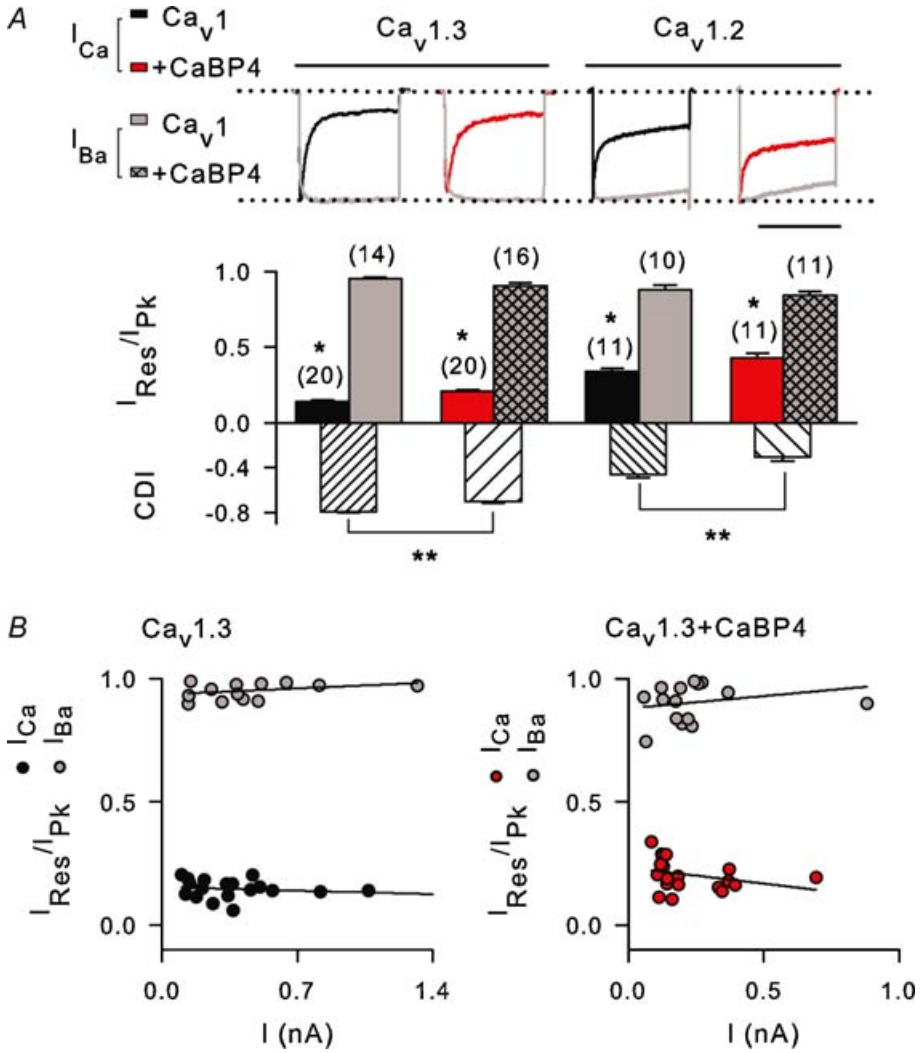

Figure 2. CaBP4 is a weak modulator of Ca_v CDI
A, inhibitory effect of CaBP4 on CDI of $Ca_v1.3$ and $Ca_v1.2$. Ca^{2+} or Ba^{2+} currents (I_{Ca}, I_{Ba}) were recorded in HEK293T cells transfected with $Ca_v1.3$ ($\alpha_1 1.3$, β_{2a}, $\alpha_2\delta$) or $Ca_v1.2$ ($\alpha_1 1.2$, β_{2a}, $\alpha_2\delta$) alone or cotransfected with CaBP4. Test pulses were 300 ms steps from −90 to −20 mV for $Ca_v1.3$ or 1 s steps from −80 to −10 mV for $Ca_v1.2$. Inactivation was measured as I_{res}/I_{pk}, which was the residual current amplitude at the end of the pulse normalized to the peak current amplitude. CDI is the difference in I_{res}/I_{pk} for I_{Ca} and I_{Ba}. Representative current traces for I_{Ca} (black or red) and I_{Ba} (grey) are shown. $^*P < 0.01$ compared to I_{Ba} by *t* test; $^{**}P < 0.005$ compared to $Ca_v1.3$ or $Ca_v1.2$ alone, by ANOVA and *post hoc* Bonferroni *t* test. Number of cells in each group indicated in parentheses. Scale bar, 0.2 s for $Ca_v1.3$ and $Ca_v1.3$ + CaBP4; 0.65 s for $Ca_v1.2$. Representative current traces are shown above. Scale bar, 800 ms for $Ca_v1.2$, 250 ms for $Ca_v1.3$. *B*, current independence of $Ca_v1.3$ inactivation. I_{res}/I_{pk} for cells obtained in *A* was plotted against peak current amplitude for I_{Ca} and I_{Ba} in cells transfected with $Ca_v1.3$ alone (left) or cotransfected with CaBP4 (right). Each point represents I_{res}/I_{pk} for a single cell. Data were linear as determined by Run's test, with regression line indicated. For both $Ca_v1.3$ alone and $Ca_v1.3$ + CaBP4, the slopes of the regression line did not differ significantly from zero (for $Ca_v1.3$ alone, $P = 0.08$ for I_{Ca}, $P = 0.28$ for I_{Ba}; for $Ca_v1.3$ + CaBP4, $P = 0.58$ for I_{Ca}, $P = 0.29$ for I_{Ba}; by ANOVA).

Table 1. Current-densities measured in cells transfected with $Ca_v1.3 \pm$ CaBPs

Transfection	Current-density (pA pF^{-1})	*P* value	*n*
$Ca_v1.3\ \beta_1$	48.3 ± 10.1	—	9
+ CaBP4	36.8 ± 10.5	0.44	9
+ CaBP1	23.9 ± 6.3	0.05	10
+ CaBP2	28.9 ± 7.3	0.13	12
+ CaBP5	25.2 ± 8.6	0.08	12
$Ca_v1.3\ \beta_2$	30.0 ± 6.9	—	20
+ CaBP4	14.7 ± 2.3	0.03	20
$Ca_v1.3\ \beta_3$	28.8 ± 4.3	—	9
+ CaBP4	16.9 ± 4.9	0.09	9
$Ca_v1.3\ \beta_4$	39.8 ± 7.9	—	12
+ CaBP4	32.2 ± 6.9	0.48	12

it was possible that CaBP4 inhibited CDI indirectly via secondary effects on channel density. If so, then as shown for Ca_v2 channels (Kreiner & Lee, 2006; Soong *et al.* 2002), inactivation of $Ca_v1.3$ I_{Ca}, but not I_{Ba}, should increase nonlinearly with whole-cell current amplitude. In addition, CaBP4 would not change the parameters of this relationship, but rather the range of current amplitudes sampled. In this case, the mean value for I_{res}/I_{pk} for I_{Ca} in cells with $Ca_v1.3$ + CaBP4 would be greater than that in cells transfected with $Ca_v1.3$ alone since smaller currents show less CDI. However, in cells transfected with $Ca_v1.3$ alone or cotransfected with CaBP4, inactivation of I_{Ca} and I_{Ba} did not vary significantly with current amplitude (Fig. 2*B*). For both groups, the relationship between current amplitude and I_{res}/I_{pk} was linear, with a slope not significantly different from zero. Thus, like $Ca_v1.2$ channels (Neely *et al.* 1994), CDI of $Ca_v1.3$ is independent of channel expression levels, perhaps due to a reliance on very local increases in Ca^{2+} through individual channels. This result argues against a role for the CaBP4-mediated decrease in current density in the mechanism by which CaBP4 inhibits CDI.

Because modulation of CDI can vary with the identity of the auxiliary $Ca_v\beta$ subunit (Lee *et al.* 2000), we tested if CaBP4 might have stronger effects on CDI of $Ca_v1.3$ channels comprised of different β subunits. CaBP4 caused a significant but still modest level of inhibition of I_{Ca} inactivation in channels with β_1, β_2 and β_4 without any effects on I_{Ba} (Fig. 3). Interestingly, CaBP4 did not influence inactivation of I_{Ca} for $Ca_v1.3$ channels containing β_3. In contrast to the stimulatory effects of CaBP4 on voltage-dependent activation of $Ca_v1.4$ (Haeseleer *et al.* 2004), CaBP4 did not similarly influence $Ca_v1.3$ channels, regardless of $Ca_v\beta$ (Table 2). In addition, the negative effects of CaBP4 on current density were significant only for $Ca_v1.3$ channels containing $Ca_v\beta_2$ (Table 1). These data indicate that CaBP4 differentially modulates $Ca_v1.3$ compared to $Ca_v1.4$, and has weak modulatory effects on CDI for $Ca_v1.3$ containing most $Ca_v\beta$ subunits.

Normal hair cell synaptic transmission in mice lacking CaBP4

To address the significance of CaBP4 as a modulator of auditory $Ca_v1.3$ channels, we tested if the absence of CaBP4 affected CDI of IHCs and sound coding at the IHC afferent synapses. Patch-clamp recordings of IHCs in the apical coil of the organ of Corti monitored I_{Ca} and exocytic membrane capacitance changes (ΔC_m) reflecting neurotransmitter release (Moser & Beutner, 2000) from wild-type (WT, C57Bl/6) and CaBP4$^{-/-}$ mice. As predicted from our results in transfected cells (Figs 2 and 3), CDI was marginally, but significantly enhanced (from −0.08 in WT to −0.13 in CaBP4$^{-/-}$ IHCs, $P = 0.036$), while inactivation of I_{Ba} was not affected in CaBP4$^{-/-}$ IHCs ($P = 0.553$; Fig. 4*A*–*C*). In addition, voltage-dependent activation and peak amplitudes of I_{Ca}

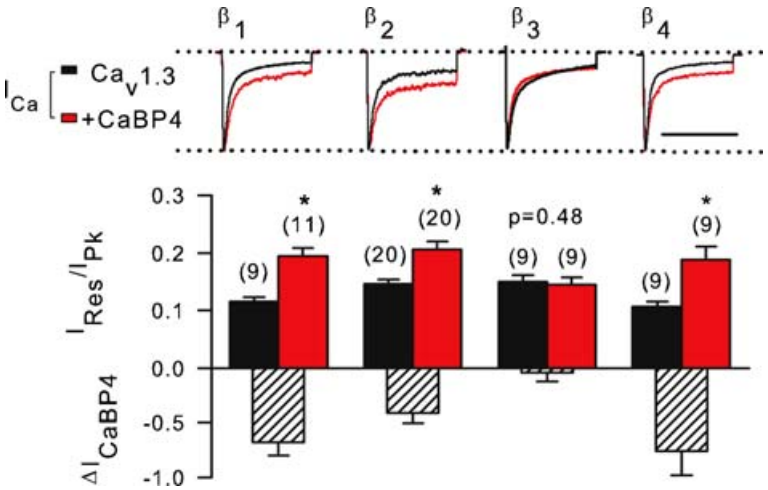

Figure 3. Weak modulation by CaBP4 is independent of $Ca_v\beta$ subunit
I_{res}/I_{pk} was determined for I_{Ca} as in Fig. 2*A* in cells cotransfected with $Ca_v1.3$ ($\alpha_1$1.3, β, $\alpha_2\delta$) alone or cotransfected with CaBP4. Inhibition of inactivation by CaBP4 was measured as $\Delta I_{CaBP4} = [(I_{res}/I_{pk}$ for $Ca_v1.3) - (I_{res}/I_{pk}$ for $Ca_v1.3$ + CaBP4)]/(I_{res}/I_{pk} for $Ca_v1.3$). *$P < 0.02$ compared to $Ca_v1.3$ alone by *t* test. Representative current traces are shown above. Scale bar, 250 ms. Number of cells indicated in parentheses.

Table 2. Parameters for activation of $Ca_v1.3$ from *I–V* relationships

Transfection	$V_{1/2}$ (mV)	*P* value	*k*	*P* value	*n*
I_{Ba}					
$Ca_v1.3\ \beta_1$	-15.35 ± 1.86		-6.77 ± 0.32		10
+ CaBP4	-17.60 ± 1.87	0.40	-6.97 ± 0.47	0.73	8
$Ca_v1.3\ \beta_2$	-13.55 ± 1.35		-8.52 ± 0.18		10
+ CaBP4	-10.02 ± 1.09	0.058	-8.71 ± 0.23	0.53	10
$Ca_v1.3\ \beta_3$	-14.05 ± 2.25		-9.90 ± 0.63		10
+ CaBP4	-13.36 ± 2.07	0.83	-7.53 ± 0.50	0.01	7
$Ca_v1.3\ \beta_4$	-17.28 ± 1.87		-7.23 ± 0.29		9
+ CaBP4	-14.58 ± 1.77	0.78	-7.09 ± 0.24	0.72	9
I_{Ca}					
$Ca_v1.3\ \beta_1$	-7.31 ± 0.66		-7.44 ± 0.37		10
+ CaBP4	-7.32 ± 0.86	0.99	-7.80 ± 0.23	0.42	12
$Ca_v1.3\ \beta_2$	-6.86 ± 1.09		-8.43 ± 0.31		10
+ CaBP4	-6.55 ± 1.04	0.84	-8.84 ± 0.28	0.33	12
$Ca_v1.3\ \beta_3$	-5.44 ± 0.73		-8.73 ± 0.21		9
+ CaBP4	-7.29 ± 1.63	0.33	-8.39 ± 0.35	0.41	7
$Ca_v1.3\ \beta_4$	-8.68 ± 1.44		-7.39 ± 0.39		11
+ CaBP4	-8.23 ± 0.75	0.31	-8.31 ± 0.33	0.085	12

were not different in WT and $CaBP4^{-/-}$ IHCs (data not shown). As expected, analyses of I_{Ca} integrals and ΔC_m (Fig. 4*D* and *E*) revealed that Ca^{2+} influx and exocytosis were comparable in $CaBP4^{-/-}$ and WT IHCs for depolarizations up to 200 ms (Fig. 4*D* and *E*).

Consistent with these findings, we found normal auditory brainstem responses (ABR) to click or short tone burst stimuli in $CaBP4^{-/-}$ mice. ABR waveforms (Fig. 4*F*), latencies (data not shown) and thresholds (Fig. 4*G*) were not different from WT mice. Distortion product otoacoustic emissions were also unaltered in $CaBP4^{-/-}$ mice, indicating intact cochlear amplification (data not shown). These findings confirm that CaBP4 is a relatively modest suppressor of $Ca_v1.3$ CDI in IHCs, but is not essential for normal IHC development and IHC function in auditory transduction.

CaBP1 is a candidate modulator of $Ca_v1.3$ CDI in IHCs

To explore alternative mechanisms for inhibiting CDI in IHCs, we assessed the expression other CaBP isoforms by immunohistochemistry in the mouse organ of Corti. In addition to that for CaBP4, immunolabelling for CaBP1, CaBP2 and CaBP5 was detected in IHCs (Fig. 5*A–C*). The specificity of the immunostaining was supported by the substantial reduction of signal upon preadsorption of the CaBP antibodies with the corresponding immunogen (Supplemental Fig. 1*b*). The expression of CaBP1, CaBP2 and CaBP4 in cochlear extracts was confirmed by RT-PCR analysis (Fig. 5*D*). However, CaBP5 was not detected by this method perhaps due to the low expression levels of CaBP5 relative to other CaBPs in IHCs. Interestingly, CaBP1 showed a punctate distribution at the base of IHCs from older mice (P28, data not shown, and 2 months old; Fig. 5*E*) in contrast to the diffuse localization of CaBP1 in IHCs from younger mice (P14; Fig. 5*A*). The CaBP1-labelled puncta strongly colocalized with labelling for CtBP2. These data suggested the likely colocalization of CaBP1 with presynaptic $Ca_v1.3$ channels, which show a similar subcellular distribution (Brandt *et al.* 2005). The presynaptic localization of CaBP1 was qualitatively similar in $CaBP4^{-/-}$ IHCs (Fig. 5*E*, lower panels). If CaBP1 more prominently suppressed CDI of $Ca_v1.3$ in IHCs, CaBP1/$Ca_v1.3$ interactions could explain the relatively normal auditory phenotype in $CaBP4^{-/-}$ mice.

To test this, we compared the capacities of CaBP1, 2 and 5 as modulators of $Ca_v1.3$ CDI in transfected HEK293T cells. While CaBP5 had modest effects on CDI that were not significantly different from those of CaBP4 ($P = 0.94$), CaBP2 had no impact in this regard ($I_{res}/I_{pk} = 0.14 \pm 0.01$ for + CaBP2 *versus* 0.12 ± 0.01 for $Ca_v1.3$ alone; $P = 0.42$; Fig. 6). However, CaBP1 caused a significantly stronger suppression of CDI than CaBP4 ($P < 0.001$; Fig. 6). Similar to CaBP4, CaBP1 interacted with the NT and CT of $\alpha_1 1.3$ in a Ca^{2+}-independent manner in pull-down assays (Fig. 7*A*). Thus, while CaBP1 and CaBP4 may bind to the same sites in $\alpha_1 1.3$, they exhibit distinct modulatory strengths with respect to inactivation of I_{Ca}.

Our electrophysiological results could also be explained by differences in the relative expression levels and/or transfection efficiency of CaBP1 and CaBP4. To address these possibilities, we performed Western blot analyses of lysates of cells transfected with $Ca_v1.3$ alone or cotransfected with CaBP1 or CaBP4. To control for differences in immunoblotting efficiencies of CaBP1 and CaBP4 antibodies, signals were qualitatively compared to those corresponding to known quantities of the

purified proteins. With this approach, we consistently observed lower levels of CaBP4 than CaBP1 in transfected cell lysates (Fig. 7*B*). However, when GFP-tagged CaBP1 or CaBP4 constructs were cotransfected with $Ca_v1.3$ as for electrophysiological experiments, we did not find significantly weaker transfection efficiency of CaBP4 compared to CaBP1 (Fig. 7*C* upper panels). We did note that GFP-CaBP4 fluorescence was generally weaker and

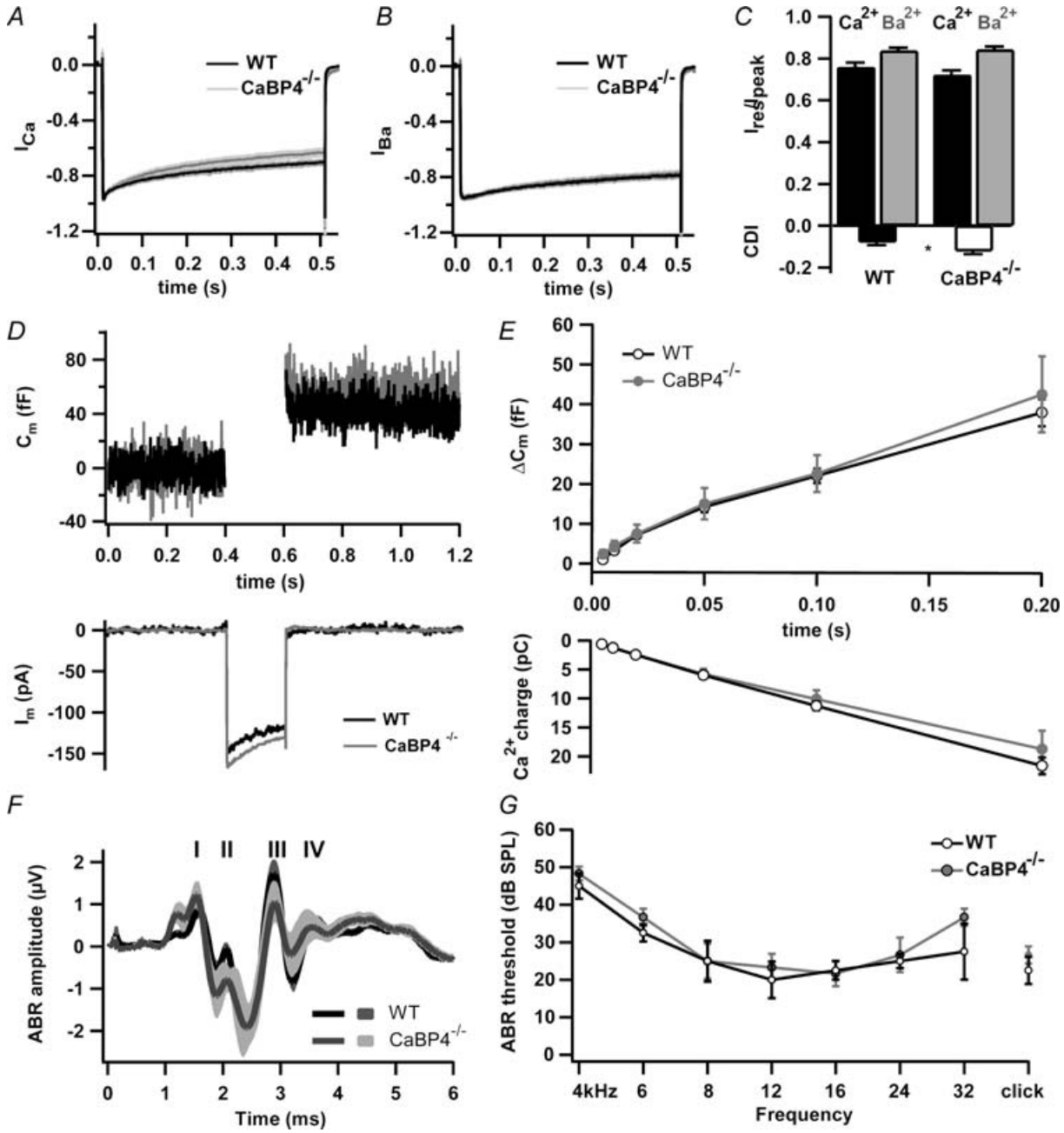

Figure 4. Hearing is not impaired in CaBP4 knockout mice
A and *B*, mean I_{Ca} (*A*) and I_{Ba} (*B*) of WT (black, $n = 12$) and CaBP4$^{-/-}$ (grey, $n = 14$) IHCs evoked by 500 ms depolarizations to −16 mV. Currents were normalized to their peak amplitude and displayed with standard errors. *C*, I_{res}/I_{pk} and CDI were determined as in Fig. 2*A* except that currents were evoked as in (*A* and *B*) and residual current amplitude was measured at 300 ms. *D*, representative I_{Ca} and baseline-subtracted C_m traces (200 ms step to −16 mV). *E*, grand average of ΔC_m (top) and I_{Ca} integrals (bottom) plotted against pulse duration for WT ($n = 25$) and CaBP4 $^{-/-}$ ($n = 7$) IHCs. *F*, grand average of ABR evoked by suprathreshold clicks (80 dB) in WT (black) and CaBP4$^{-/-}$ mice (grey). Roman numerals denominate the individual ABR peaks arising from the neurons of the ascending auditory pathway. *G*, ABR audiograms of WT (black) and CaBP4$^{-/-}$ mice (grey) obtained by tone burst and click stimulation.

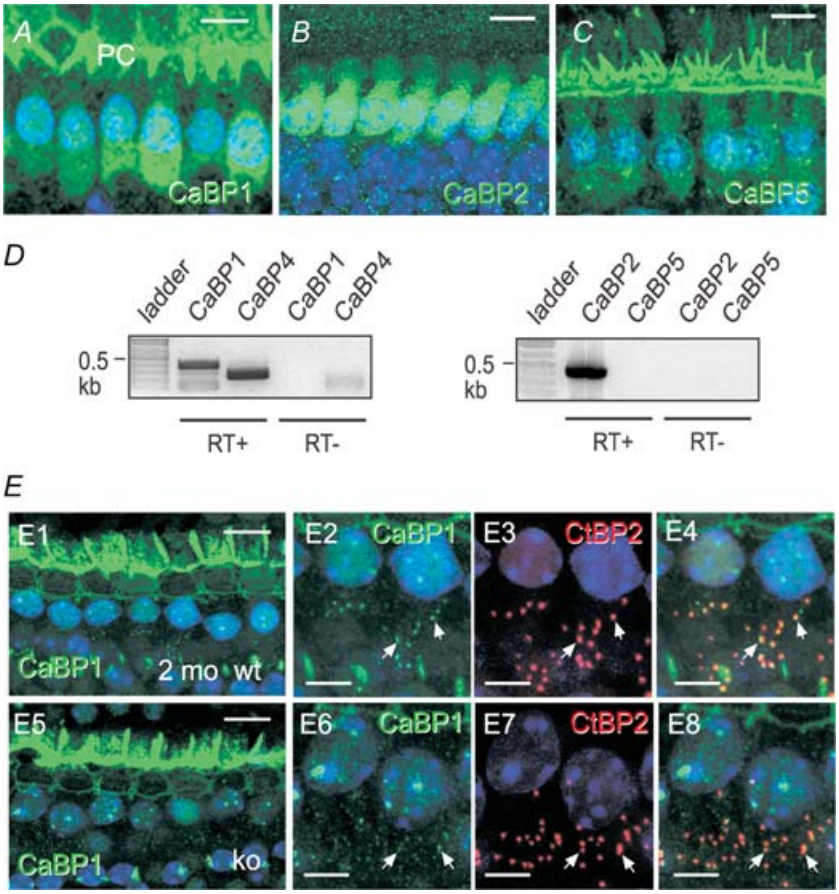

Figure 5. CaBP1, 2, and 5 are localized in IHCs
A–C, confocal micrographs of whole-mount preparations of mouse organ of Corti (P14–P15) labelled with antibodies against CaBP1 (*A*), CaBP2 (*B*), or CaBP5 (*C*) and FITC-secondary antibodies (green) followed by Hoechst staining of nuclei (blue). Images represent single (*A*), or projections of, confocal section(s) (*B* and *C*). CaBP1 staining was detected in IHC soma and overlying pillar cells (PC). Scale bars, 10 μm. Results shown are representative of experiments performed with at least 6 organs of Corti. *D*, RT-PCR analysis of CaBP variants in mouse cochlear extracts. Reactions were performed with (+RT) or without reverse transcriptase (−RT) as a negative control. *E*, presynaptic localization of CaBP1 in IHCs from 2-month-old WT and CaBP4$^{-/-}$ (KO) IHCs. Confocal micrographs show whole-mounts of organs of Corti double labelled with antibodies against CaBP1 (green, E1, 2, 5, 6) and CtBP2 (red, E3, E7). Examples of colocalization are indicated with arrows and appear yellow in the merged images (E4, 8). Scale bars, 10 μm in E1, E2; 5 μm in E2−4, E6 −8. Results shown are representative of experiments performed with 4 organs of Corti.

diffusely localized, in contrast to the strong localization of GFP-CaBP1 at the plasma membrane (Fig. 7*C*, lower panels). These results suggest that the weak effects of CaBP4 in modulating $Ca_v1.3$ could be influenced by limited cell-surface targeting and/or lower expression levels of CaBP4 compared to CaBP1 in transfected cells.

Differential modulation of $Ca_v1.3$ CDI by CaBP4 and CaBP1

The distinct effects of CaBP1 and CaBP4 could also be mediated by separate molecular determinants for each in the NT or CT of $\alpha_1$1.3. If so, then alterations in the NT or CT should differentially affect modulation by CaBP1 and CaBP4. To test this, we initially deleted portions of the NT from $\alpha_1$1.3, since similar deletions in $\alpha_1$1.2 abolished modulation of $Ca_v1.2$ by CaBP1 (Zhou *et al.* 2005). Small and large deletions of the $\alpha_1$1.3 NT resulted in non-functional channels, which precluded functional analyses of this region. Therefore, we focused our efforts on the $\alpha_1$1.3 CT and substituted the isoleucine with glutamate in the IQ domain in the CT, since similar mutations in $\alpha_1$1.2 inhibit binding and modulation of $Ca_v1.2$ by CaBP1 (Zhou *et al.* 2004, 2005). Consistent with the essential role of the IQ domain in transducing CDI of Ca_v1 channels (Peterson *et al.* 1999; Zühlke *et al.* 1999;

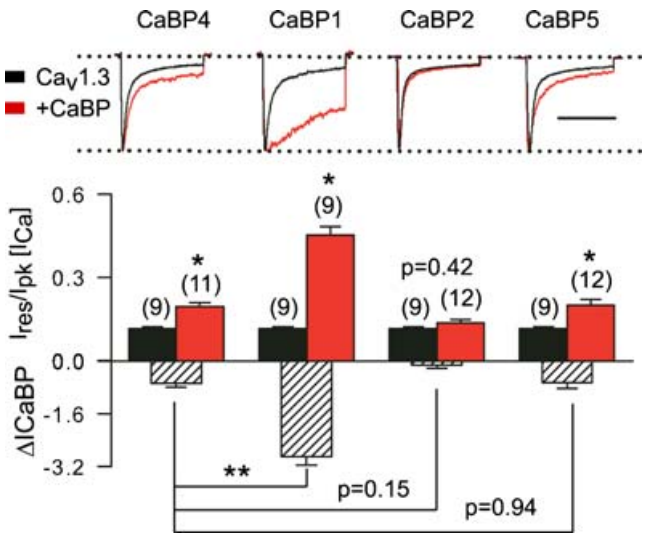

Figure 6. CaBP1 causes robust suppression of I_{Ca} inactivation compared to other CaBP variants
Distinct effects of CaBP1, 2, 4 and 5 on inactivation of $Ca_v1.3$ in transfected HEK293T cells. Measurements of I_{Ca}, I_{res}/I_{pk}, and ΔI_{CaBP} were as in Fig. 3 for cells transfected with $Ca_v1.3$ ($\alpha_1$1.3, β_{2a}, $\alpha_2\delta$) alone or cotransfected with CaBP1, 2, 4, or 5. $^*P < 0.02$ compared to $Ca_v1.3$ alone by *t* test. $^{**}P < 0.001$ compared to CaBP4 by ANOVA and *post hoc t* test. Number of cells indicated in parentheses.

Qin *et al.* 1999), the I-E mutation disrupted, although not completely, CDI of $Ca_v1.3$ ($Ca_v1.3$I-E, Fig. 8*A*). In addition, GST-tagged CT fusion proteins containing the I-E mutation showed weaker binding to CaBP4 and CaBP1 in pull-down assays (Fig. 8*B*), which suggested that $Ca_v1.3$I-E would show limited regulation by these CaBPs.

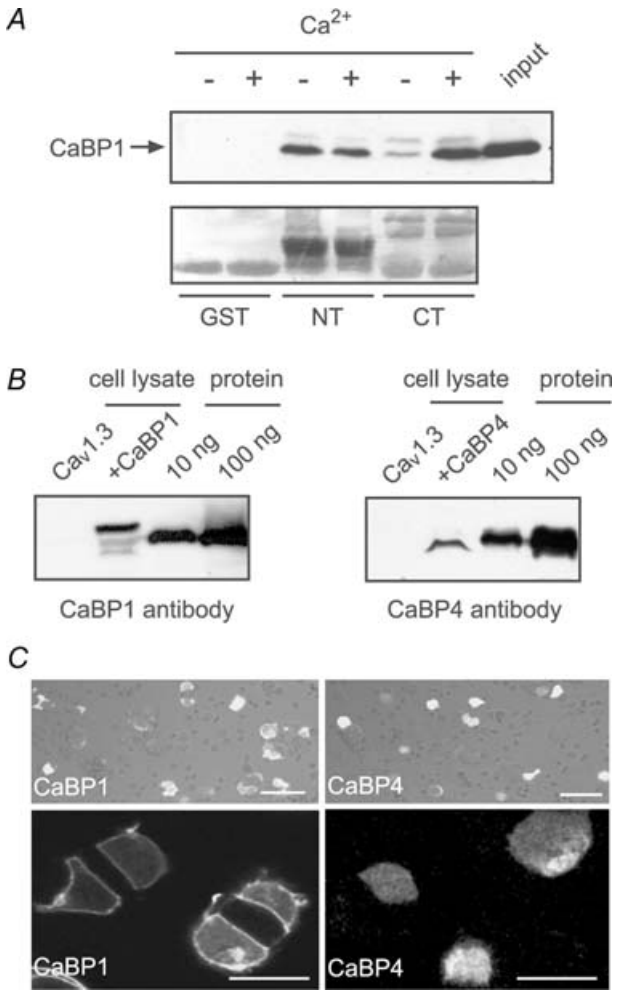

Figure 7. CaBP1 binds to same sites in $\alpha_1$1.3, but shows stronger expression levels and cell-surface targeting compared to CaBP4

A, CaBP1 pull-down with GST-tagged CT or NT performed in the presence (+) or absence (−) of Ca^{2+} as in Fig. 1*D*. Results shown are representative of 3 experiments. *B*, Western blot of lysates from cells used for electrophysiological recording shows decreased levels of CaBP4 compared to CaBP1 in cells cotransfected with Cav1.3. Lanes 1 and 2 represent lysates of cells transfected with $Ca_v1.3$ alone (lane 1) or cotransfected with CaBP (lane 2). Lanes 3 and 4 contain purified GST-tagged CaBP1 (left panel) or His-tagged CaBP4 (right panel) at the indicated quantities. Western blotting was with CaBP1 or CaBP4 antibodies. Results shown are representative of 3 experiments. *C*, confocal micrographs of GFP-tagged CaBP1 or CaBP4 cotransfected with $Ca_v1.3$ as for electrophysiological experiments. Top panels show fluorescence images overlaying DIC image (scale bars, 50 μm). Higher magnification views in lower panels reveal GFP fluorescence restricted to the plasma membrane of cells cotransfected with GFP-CaBP1 (left) as compared to diffuse localization of GFP-CaBP4 (scale bars, 20 μm). Results shown are representative of 3 experiments.

While $Ca_v1.3$I-E channels were completely insensitive to modulation by CaBP4 (Fig. 9*A* and *B*), there were residual effects of CaBP1 in that I_{Ca} inactivated ∼2 times less in cells transfected with $Ca_v1.3$I-E + CaBP1 than with $Ca_v1.3$ alone ($P < 0.001$; Fig. 9*C*).

Unexpectedly, and in contrast to CaBP4, CaBP1 significantly inhibited voltage-dependent inactivation (VDI) exhibited by I_{Ba} (∼36% compared to $Ca_v1.3$ alone, $P < 0.001$). In these experiments, CaBP regulation of VDI was probed with channels containing the Ca_v β_1 subunit, which show more prominent VDI than those with Ca_v β_2 (compare Fig. 9*B* to Fig. 2*A*). The effect of CaBP1 on VDI was completely spared by the I-E mutation ($P = 0.23$ for $Ca_v1.3$ *versus* $Ca_v1.3$I-E; Fig. 9*D*). During longer depolarizations (1 s), the inhibitory effect of CaBP1 on VDI was particularly apparent. While CaBP4 had no effect on inactivation of I_{Ba} ($I_{res}/I_{pk} = 0.29 \pm 0.03$ for $Ca_v1.3$ + CaBP4 *versus* 0.34 ± 0.03 for $Ca_v1.3$ alone; $P = 0.86$), CaBP1 caused I_{Ba} to inactivate significantly less than in cells transfected with $Ca_v1.3$ alone or cotransfected with CaBP4 (Fig. 9*E*). These data reveal distinct molecular mechanisms by which CaBP1 and CaBP4 regulate $Ca_v1.3$ inactivation: while required for effects of CaBP4 on I_{Ca}, the IQ domain is necessary but not sufficient for the full modulation of I_{Ca} and I_{Ba} by CaBP1.

Discussion

Our study provides new insights into the physiological roles of CaBPs as integral subunits and modulators of Ca_v channels. First, CaBPs are not equally effective modulators of CDI. Second, CaBP4 and CaBP1 differ in how they suppress inactivation of $Ca_v1.3$: CaBP4 moderately limits inactivation of I_{Ca} through interactions with the $\alpha_1$1.3 IQ domain, while CaBP1 strongly inhibits inactivation of I_{Ca} and I_{Ba} through interactions with the IQ domain and some other region, perhaps the NT, of $\alpha_1$1.3. Third, CaBP4 contributes to, but alone does not account for, the unusually slow inactivation of $Ca_v1.3$ I_{Ca} in IHCs. The dispensability of CaBP4 for auditory function most likely results from additional modulation of $Ca_v1.3$ by CaBP1 and potentially other CaBPs, which are localized with CaBP4 in IHCs. Differential modulation of $Ca_v1.3$ by CaBPs may endow IHCs with a diverse repertoire of Ca^{2+} signals that may fine-tune transmission of acoustic stimuli.

Our results extend but also differ from those of Yang *et al.* (2006), who found that CaBP4 and CaBP1 both abolished CDI of $Ca_v1.3$ channels in transfected HEK293 cells. We employed the long variant of $\alpha_1$1.3 with exon 42, which contains an additional ∼500 amino acids downstream of the IQ domain compared to the shorter $\alpha_1$1.3 variant with exon 42A (Xu & Lipscombe, 2001) used by Yang *et al.* However, we did not find significant differences in CaBP modulation of $Ca_v1.3$ containing these $\alpha_1$1.3 variants (data

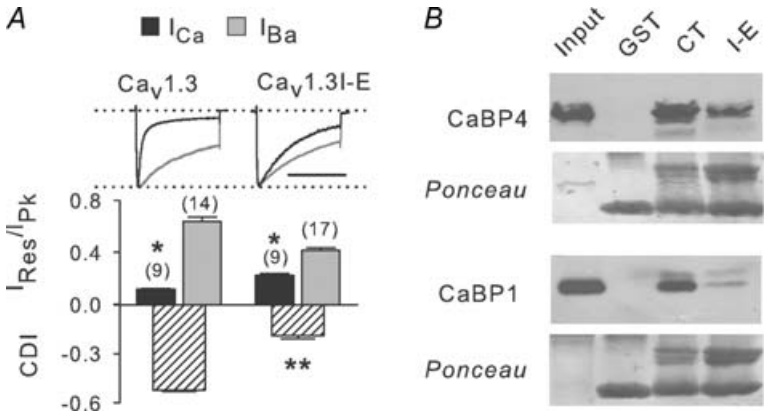

Figure 8. Mutation of the IQ domain in $\alpha_1$1.3 inhibits CDI and binding of CaBP1 and CaBP4
A, effect of I-E mutation on CDI. HEK293T cells were transfected with wild-type $Ca_v1.3$ or channels containing $\alpha_1$1.3 with I-E substitution in IQ domain ($+\beta_{1b}$, $\alpha_2\delta$). Same analysis as in Fig. 2*A* for CDI. $^*P < 0.001$ compared to I_{Ba}; $^{**}P < 0.001$ compared to $Ca_v1.3$; by *t* test. Number of cells indicated in parentheses. *B*, effect of I-E mutation on CaBP binding. Pull-down of CaBP1 or CaBP4 by GST, CT, or CT containing I-E mutation was performed as in Fig. 7*A*. Results shown are representative of 3 experiments.

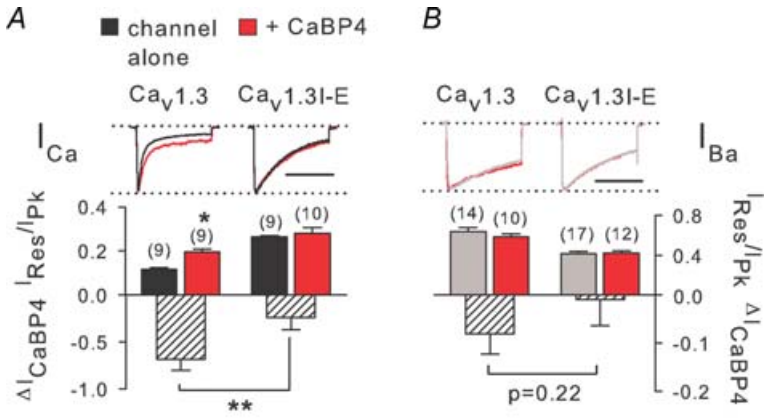

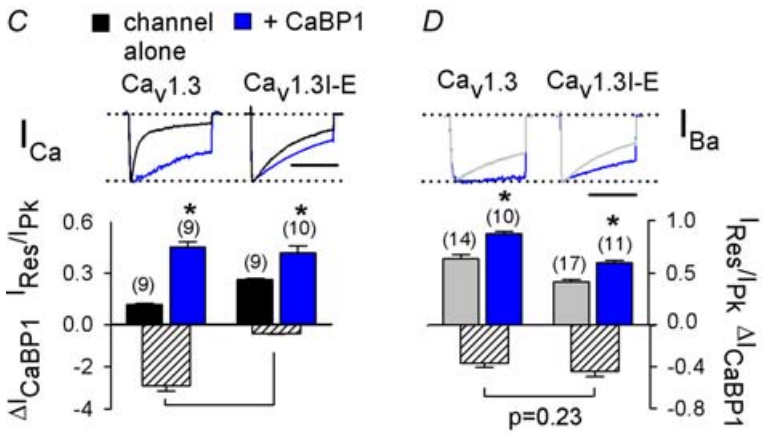

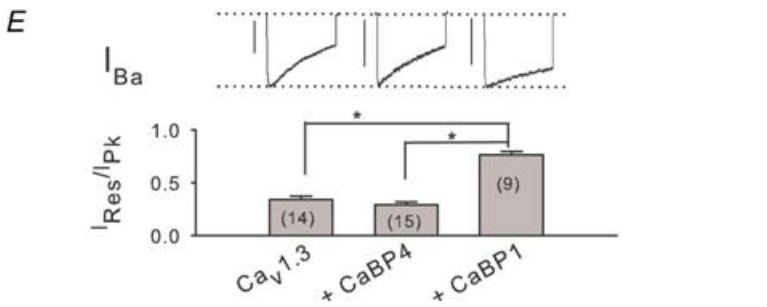

Figure 9. I-E mutation in $\alpha_1$1.3 blocks effects of CaBP4 but partially spares modulation by CaBP1
A and *B*, loss of CaBP4 effects on inactivation of $Ca_v1.3$I-E. HEK293T cells were cotransfected with CaBP4 and $Ca_v1.3$ or $Ca_v1.3$I-E ($\alpha_1$1.3 or $\alpha_1$1.3I-E, β_{1b}, $\alpha_2\delta$). Same analysis as in Fig. 3 for inactivation of I_{Ca} (*A*) and I_{Ba} (*B*). By *t* test, $^*P < 0.02$ compared to $Ca_v1.3$ alone; $^{**}P < 0.001$ compared to $Ca_v1.3$. *C* and *D*, effects of CaBP1 on inactivation are partially spared in $Ca_v1.3$I-E. Cells were cotransfected with CaBP1 and $Ca_v1.3$ or $Ca_v1.3$I-E ($\alpha_1$1.3 or $\alpha_1$1.3I-E, β_{1b}, $\alpha_2\delta$). Same analysis as in *C*. $^*P < 0.01$, $^{**}P < 0.0001$ compared to $Ca_v1.3$, by *t* test. In *A*–*D*, scale bars, 200 ms. *E*, decreased VDI of I_{Ba} in cells cotransfected with CaBP1 but not CaBP1. I_{Ba} was evoked by 1 s pulses from −90 mV to −20 mV in cells transfected with $Ca_v1.3$ alone, +CaBP4, or +CaBP1. $^*P < 0.001$ by ANOVA and *post hoc* Bonferroni test. Vertical scale bars, 0.2 nA. In *A*–*E*, number of cells is indicated in parentheses.

not shown). The discrepancy may arise from the use of an inducible CaBP4 expression system in which high levels of $Ca_v1.3$ expression by transient transfection were achieved prior to induction of CaBP4 in the previous study. This method, and higher permeant ion concentrations (20 mM *versus* 10 mM in our study) during electrophysiological recordings, overcomes the inhibitory effects we have noted of CaBPs on Ca_v expression levels (Lee *et al.* 2002; Zhou *et al.* 2004). At the same time, this approach may also mask functional differences in CaBPs, which might prevail under non-saturating CaBP expression levels, such as in our experiments where $Ca_v1.3$ was transiently cotransfected with CaBP1 or CaBP4.

In transfected cells, the decreased plasma membrane targeting of CaBP4 compared to CaBP1 may limit the modulatory potential of CaBP4. Unlike CaBP4, CaBP1 is N-terminally myristoylated (Haeseleer *et al.* 2000), which may aid in its cell-surface targeting and coassembly with $Ca_v1.3$ channels. Lack of this modification may weaken CaBP4 interactions with functional $Ca_v1.3$ channels, which may negatively influence the stability and net expression levels of CaBP4 in cotransfected cells. While electrophysiological analysis with $Ca_v1.3$I-E mutants suggest fundamental distinctions in how CaBP1 and CaBP4 interact with $Ca_v1.3$ channels, we cannot rule out that differential expression/targeting of these CaBPs also contributes to their strengths as $Ca_v1.3$ modulators.

Regardless of how differences in CaBP4 and CaBP1 in IHCs influence their roles in $Ca_v1.3$ regulation, our results argue against CaBP4 as the primary regulator of $Ca_v1.3$ in IHCs. Mouse IHCs lacking CaBP4 showed only a minor increase in CDI, indicating that CaBP4 is not essential for, but may contribute to, the peculiar slow CDI of $Ca_v1.3$ channels in IHCs. This may reflect the relatively weak effects of CaBP4 as a Ca_v1 modulator and/or limited presynaptic targeting/expression levels compared to other CaBPs. The dispensability of CaBP4 for hair cell sound coding is further demonstrated by the normal auditory brainstem responses in mice lacking CaBP4. The auditory physiology of CaBP4$^{-/-}$ mice was conducted at an age when CaBP1 is strongly localized presynaptically both in WT and CaBP4$^{-/-}$ IHCs. The less intense immunolabelling of CaBP1 in adult IHCs may have been missed by Yang *et al.* leading to their conclusion that CaBP4 was the critical modulator of $Ca_v1.3$ function at later ages (Yang *et al.* 2006). The use of cryosections in the previous study may have impaired detection of punctate labelling in adult IHCs, since only a few puncta might be visible in a single IHC with this method. In our experiments, presynaptic labelling was readily apparent in an entire row of IHCs in projections of confocal micrographs. Why CaBP1 exhibits a diffuse localization in P14 IHCs and becomes presynaptically clustered at later ages is not clear, but clearly allows CaBP1 to be well-situated to modulate $Ca_v1.3$ channels.

We also note that in transfected cells, CaBP1 not only strongly suppresses CDI (inactivation of I_{Ca}) but also inhibits VDI (inactivation of I_{Ba}), which was not seen with CaBP4 (Fig. 9). This latter point is relevant since $Ca_v1.3$ currents in IHCs show dramatically slower CDI and VDI than in recombinant systems (Platzer *et al.* 2000; Koschak *et al.*, 2001). The fact that cotransfection of $Ca_v1.3$ with CaBP1 fully reproduces the native properties of $Ca_v1.3$ channels further implicates CaBP1 as a modulator of $Ca_v1.3$ in IHCs, which may support the crucial roles of $Ca_v1.3$ channels in hearing.

References

Brandt A, Khimich D & Moser T (2005). Few CaV1.3 channels regulate the exocytosis of a synaptic vesicle at the hair cell ribbon synapse. *J Neurosci* **25**, 11577–11585.

Brandt A, Striessnig J & Moser T (2003). CaV1.3 channels are essential for development and presynaptic activity of cochlear inner hair cells. *J Neurosci* **23**, 10832–10840.

Calin-Jageman I, Yu K, Hall RA, Mei L & Lee A (2007). Erbin enhances voltage-dependent facilitation of Cav1.3 Ca^{2+} channels through relief of an autoinhibitory domain in the Cav1.3 α1 subunit. *J Neurosci* **27**, 1374–1385.

Dou H, Vazquez AE, Namkung Y, Chu H, Cardell EL, Nie L, Parson S, Shin HS & Yamoah EN (2004). Null mutation of α1D Ca^{2+} channel gene results in deafness but no vestibular defect in mice. *J Assoc Res Otolaryngol* **5**, 215–226.

Haeseleer F, Imanishi Y, Maeda T, Possin DE, Maeda A, Lee A, Rieke F & Palczewski K (2004). Essential role of Ca^{2+}-binding protein 4, a Cav1.4 channel regulator, in photoreceptor synaptic function. *Nat Neurosci* **7**, 1079–1087.

Haeseleer F, Sokal I, Verlinde CL, Erdjument-Bromage H, Tempst P, Pronin AN, Benovic JL, Fariss RN & Palczewski K (2000). Five members of a novel Ca^{2+}-binding protein (CABP) subfamily with similarity to calmodulin. *J Biol Chem* **275**, 1247–12460.

Ivanina T, Blumenstein Y, Shistik E, Barzilai R & Dascal N (2000). Modulation of L-type Ca^{2+} channels by G$\beta\gamma$ and calmodulin via interactions with N and C termini of α1C. *J Biol Chem* **275**, 39846–39854.

Khimich D, Nouvian R, Pujol R, Tom Dieck S, Egner A, Gundelfinger ED & Moser T (2005). Hair cell synaptic ribbons are essential for synchronous auditory signalling. *Nature* **434**, 889–894.

Koschak A, Reimer D, Huber I, Grabner M, Glossmann H, Engel J & Striessnig J (2001). α1D (Cav1.3) subunits can form L-type Ca^{2+} channels activating at negative voltages. *J Biol Chem* **276**, 22100–22106.

Kreiner L & Lee A (2006). Endogenous and exogenous Ca^{2+} buffers differentially modulate Ca^{2+}-dependent inactivation of Cav2.1 Ca^{2+} channels. *J Biol Chem* **281**, 4691–4698.

Lee A, Scheuer T & Catterall WA (2000). Ca^{2+}/calmodulin-dependent facilitation and inactivation of P/Q-type Ca^{2+} channels. *J Neurosci* **20**, 6830–6838.

Lee A, Westenbroek RE, Haeseleer F, Palczewski K, Scheuer T & Catterall WA (2002). Differential modulation of Cav2.1 channels by calmodulin and Ca^{2+}-binding protein 1. *Nat Neurosci* **5**, 210–217.

Marcotti W, Johnson SL, Rusch A & Kros CJ (2003). Sodium and calcium currents shape action potentials in immature mouse inner hair cells. *J Physiol* **552**, 743–761.

Moser T & Beutner D (2000). Kinetics of exocytosis and endocytosis at the cochlear inner hair cell afferent synapse of the mouse. *Proc Natl Acad Sci U S A* **97**, 883–888.

Neely A, Olcese R, Wei X, Birnbaumer L & Stefani E (1994). Ca^{2+}-dependent inactivation of a cloned cardiac Ca^{2+} channel $\alpha 1$ subunit (α_{1C}) expressed in *Xenopus* oocytes. *Biophys J* **66**, 1895–1903.

Peterson BZ, DeMaria CD, Adelman JP & Yue DT (1999). Calmodulin is the Ca^{2+} sensor for Ca^{2+}-dependent inactivation of L-type calcium channels. *Neuron* **22**, 549–558.

Platzer J, Engel J, Schrott-Fischer A, Stephan K, Bova S, Chen H, Zheng H & Striessnig J (2000). Congenital deafness and sinoatrial node dysfunction in mice lacking class D L-type Ca^{2+} channels. *Cell* **102**, 89–97.

Qin N, Olcese R, Bransby M, Lin T & Birnbaumer L (1999). Ca^{2+}-induced inhibition of the cardiac Ca^{2+} channel depends on calmodulin. *Proc Natl Acad Sci U S A* **96**, 2435–2438.

Sendin G, Bulankina AV, Riedel D & Moser T (2007). Maturation of ribbon synapses in hair cells is driven by thyroid hormone. *J Neurosci* **27**, 3163–3173.

Shen Y, Yu D, Hiel H, Liao P, Yue DT, Fuchs PA & Soong TW (2006). Alternative splicing of the $Ca_v1.3$ channel IQ domain, a molecular switch for Ca^{2+}-dependent inactivation within auditory hair cells. *J Neurosci* **26**, 10690–10699.

Soong TW, DeMaria CD, Alvania RS, Zweifel LS, Liang MC, Mittman S, Agnew WS & Yue DT (2002). Systematic identification of splice variants in human P/Q-type channel $\alpha 12.1$ subunits: implications for current density and Ca^{2+}-dependent inactivation. *J Neurosci* **22**, 10142–10152.

Xu W & Lipscombe D (2001). Neuronal CaV1.3$\alpha 1$ L-type channels activate at relatively hyperpolarized membrane potentials and are incompletely inhibited by dihydropyridines. *J Neurosci* **21**, 5944–5951.

Yang PS, Alseikhan BA, Hiel H, Grant L, Mori MX, Yang W, Fuchs PA & Yue DT (2006). Switching of Ca^{2+}-dependent inactivation of $Ca_v1.3$ channels by calcium binding proteins of auditory hair cells. *J Neurosci* **26**, 10677–10689.

Zhou H, Kim SA, Kirk EA, Tippens AL, Sun H, Haeseleer F & Lee A (2004). Ca^{2+}-binding protein-1 facilitates and forms a postsynaptic complex with $Ca_v1.2$ (L-type) Ca^{2+} channels. *J Neurosci* **24**, 4698–4708.

Zhou H, Yu K, McCoy KL & Lee A (2005). Molecular mechanism for divergent regulation of $Ca_v1.2$ Ca^{2+} channels by calmodulin and Ca^{2+}-binding protein-1. *J Biol Chem* **280**, 29612–29619.

Zühlke RD, Pitt GS, Deisseroth K, Tsien RW & Reuter H (1999). Calmodulin supports both inactivation and facilitation of L-type calcium channels. *Nature* **399**, 159–162.

Acknowledgements

This work was supported by grants from the NIH (NS044922 to A.L., DC008417 to I.C.J., EY014561 to F.H.); the Deafness Research Foundation (to I.C.J. and A.L.); the DFG (Center for Molecular Physiology of the Brain), the HFSP (RGY0019), the BMBF (Bernstein Center for Computational Neuroscience Goettingen) and the EC (Eurohear) to T.M. We would like to thank C. Ruediger, M. Koeppler and A. Gonzalez (Moser Laboratory) for excellent technical assistance, G. Géléoc (U. Virginia) for advice on processing cochlear tissue, and F. Gregory (Lee Laboratory) for comments on the manuscript.

Supplemental material

Online supplemental material for this paper can be accessed at:
http://jp.physoc.org/cgi/content/full/jphysiol.2007.142307/DC1
and
http://www.blackwell-synergy.com/doi/suppl/10.1113/jphysiol.2007.142307